Research Article | Vol. 1, No. 3 | 15 Nov 2018 | OSA CONTINUUM 1041
OSA CONTINUUM

Effect of illuminating wavelength on the contrast of meibography images

ASSUMPTA PERAL,[1] JOSE ALONSO,[2,3] AND JOSE A. GOMEZ-PEDRERO[2,*]

[1]*Department of Optometry and Vision, Universidad Complutense de Madrid, Facultad de Óptica y Optometría, C/ Arcos de Jalón, 118, 28037, Madrid, Spain*
[2]*Applied Optics Complutense Group, Optics Department, Universidad Complutense de Madrid, Facultad de Óptica y Optometría, C/ Arcos de Jalón, 118, 28037, Madrid, Spain*
[3]*Indizen Optical Technology, C/ Santa Engracia, 6, 28010, Madrid, Spain*
**jagomezp@ ucm.es*

Abstract: Evaluation of the Meibomian glands morphology is becoming a popular assessment for dry eye. This evaluation is usually done by imaging the glands on the everted lids while they are illuminated with infrared light. Nowadays techniques to determine gland condition and dropout are based on grading scales with which meibography images are subjectively evaluated. In this work, we have measured the contrast of Meibomian gland images from ten subjects and for a range of wavelengths of the monochromatic illuminating light. We have used a xenon lamp and a monochromator as a light source, and a semi-automatic image processing technique for measuring the image contrast from 600 nm to 1050 nm. Contrast values inside glands are from 0.025 to 0.015 and between glands from 0.06 to 0.04. The greater values of contrast are obtained when Meibomian glands are illuminated with a wavelength close to 600 nm.

1. Introduction

The interest in the study of Meibomian glands has become more relevant in the last years. The main reason is that alteration of these glands seems to be highly correlated with dry eye. Meibomian glands are modified sebaceous glands located into the tarsal plates of the eyelids. An elongated central duct surrounded by grape-like structures called acini forms these glands. These acini are filled with secretory meibocites that produce and secrete a lipidic substance called meibum into the tears [1]. Some authors [2,3] suggest that meibum plays an important role in affecting the surface tension of the tear film and avoiding a quick evaporation rate of the tears, although the exact role of the meibum in the tear film is still under research [4,5]. When Meibomian glands are altered, which is known by Meibomian Gland Dysfunction (MGD), a stasis in the meibum inside the glands is produced followed by a dilatation of the ductal system and the loss of glandular tissue also identified as gland dropout [6].

MGD is a common abnormality in ophthalmic practice that leads to an alteration of the tear film lipid layer [7] and to evaporative dry eye [6–10]. MGD has been defined as a chronic, diffuse abnormality of Meibomian glands, commonly characterized by terminal duct obstruction and /or qualitative/quantitative changes in the glandular secretion. This may result in alteration of the tear film, symptoms of eye irritation, clinically apparent inflammation, and ocular surface disease [11].

Due to the implications of this alteration, different techniques have been developed to observe and assess Meibomian glands. These procedures include slit lamp microscopy with visible light and meibography with infrared light (IR), as the most commonly used techniques to evaluate the health of the glands. Meibography is a specialized imaging study developed for visualizing the morphology of Meibomian glands in vivo [12–16]. There are currently two different types of meibography, trans-illumination of the everted eyelid [17–19] and direct illumination also known as non-contact meibography [20–23].

#338104 https://doi.org/10.1364/OSAC.1.001041
Journal © 2018 Received 6 Jul 2018; revised 5 Oct 2018; accepted 11 Oct 2018; published 13 Nov 2018

OSA CONTINUUM

Tapie firstly used the trans-illumination technique in 1977 with a red light filter illumination probe inserted behind the everted eyelid and a slit lamp to observe Meibomian glands [12], afterward an IR light source was used to do the visualization [17,24]. This procedure showed disadvantages like heating discomfort and pain reports from patients, the difficulty of capturing images from the entire eyelid due to the small trans-illumination area and a process of capturing IR images limited to IR cameras [17].

Arita et al. introduced the non-contact meibography technique in 2008 [20]. This system combines a slit lamp biomicroscope with an IR filter (830 nm), and an IR charge-coupled device (CCD) video camera to image the Meibomian glands from the everted eyelid [20]. This technique does not need an illumination probe, and that increases the comfort of the patients during the exam. Pult et al. developed another non-contact device in 2011 [25], consisting of a modified IR security camera (802CHA CCD; Shenzhen LYD Technology Co. Ltd, Shenzhan, China). This IR CCD video-camera incorporates an IR light source which is aimed to the everted eyelid which is then imaged and captured to analyze it. Srinivasan et al. reported the use of the topographer Keratograph 4 (OCULUS, Wetzlar, Germany and JenVis Research –Jena, Germany-) to perform meibography in 2012 [26]. The illuminating wavelength of Keratograph 4 is 880 nm. Since then, other instruments based on IR light have been used for this purpose. Recently, Napoli et al. [27] propose the usage of an Optical Coherent Tomography (OCT) technique to evaluate Meibomian glands showing its advantages against conventional imaging techniques. In this work, Napoli et al. used image processing technique to enhance the contrast and brightness of OCT images (taken at a wavelength of 840 nm) so the microscopic structures of the glands could be highlighted. The main drawback of this technique is the availability of such an expensive equipment as an OCT scanner to an average practitioner.

The visualization of the glands essentially permits obtaining information about their number, their partial or total loss, their thickness and tortuosity and even the bent angle they show along the eyelid. There are several grading scales to score all these aspects but there are no agreed and established standards in the classification of Meibomian glands [19,20,25,28–32]. In the last years, automatic techniques for detecting the inner structure of the glands [33,34] and assessing the glands [35] from gland images taken with Keratograph 5 (OCULUS) with an illuminating wavelength of 840 nm have appeared in the literature.

In Table 1 we have summarized the illuminating wavelength used in some of the studies mentioned above. From this table we can infer that non-contact meibography is usually performed with an illuminating wavelength close to 840 nm.

Table 1. Illuminating Wavelengths Employed in Different Studies of Meibomian Glands

Authors	Reference	Year	Technique	Wavelength (nm)
Yokoi et al.	[17]	2007	Trans-illumination	850
Arita et al.	[20]	2008	Slit lamp observation	830
Srivasan et al.	[26]	2012	Keratograph 4	880
Napoli et al.	[27]	2016	OCT	840
Koprowski et al.	[34]	2016	Keratograph 5	840

It seems clear that meibography is a powerful and simple technique to assess the condition of the Meibomian glands but the images usually lack good contrast and may be difficult to analyze. Because of this, optimization of the imaging system should be sought. It is also important to determine whether it is possible to use red light instead of infrared one, as this would make possible the usage of cheaper and simpler setups to take the images and grading the Meibomian glands, either manual or automatically. The present study shows the relationship between the contrast of the Meibomian gland image and the visible and infrared illuminating wavelengths employed in the imaging process. It also gives some clues of which wavelengths gives higher contrast of the Meibomian gland images. A hypothesis to be tested in subsequent works is whether this contrast can provide the practitioner with an extra

OSA CONTINUUM

objective parameter to improve over the current graduated scales in the evaluation of the pathology of the glands.

2. Material and methods

The present study was conducted in accordance with the Helsinki Declaration guidelines and was approved by the Independent Research Ethics Committee of the Clinic Hospital San Carlos of Madrid (favorable judgment C.P.-C.I. 15/518-E.). The study was carried out with ten subjects who were provided with informed consent that they accepted. Only the right eye of each subject was measured. In order to avoid experimental complexity, we chose subjects with healthy eyes without any problems on the ocular surface. They were not contact lens users.

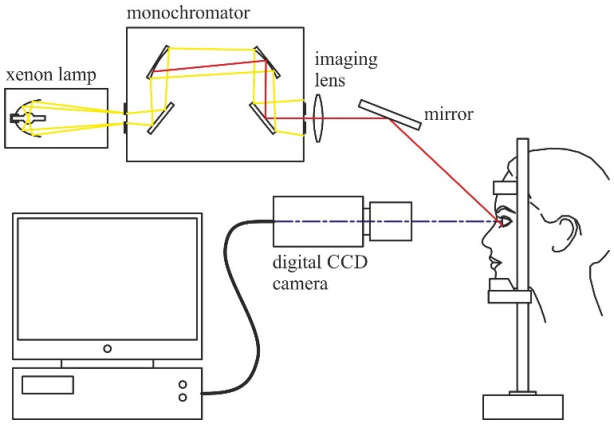

Fig. 1. Experimental set-up used for imaging the Meibomian glands with tunable monochromatic light.

The experimental set up is shown in Fig. 1. We have imaged Meibomian glands of the everted lower right lid of each subject using a digital CCD camera iNET-GmbH model NS1130BU fitted with a Navitar lens NMV-6WA with focal length 25 mm, and maximum aperture F/1.4. Distance from the everted lid to the first rim of the lens was 10 cm, and, at this object distance, magnification yielded 74.0 ± 0.7 pixels/mm.

The measurements were made in a refraction room with general lightning turned off, and illuminating the eye with the monochromatic light coming from a double grating monochromator PTI SID101 to which white light from a 75 Watts xenon lamp PTI A-1010B was injected. Monochromator slits were adjusted so that the FWHM (full width a half height) of the output light was 2 nm, as measured with a fiber spectrometer AvaSpec ULS2048-USB2-VA-50, (Avantes, Apledoorn, The Netherlands.) The same spectrometer was used to calibrate the manual dial of the monochromator. Maximum wavelength error in the measured spectral region was smaller than 0.3 nm.

The light from the monochromator output slit was collimated with a cylindrical lens and, by means of a plane mirror, directed to the subject's eye at an angle of 20° with respect to the axis of the imaging optics. Images of the everted lid were taken in steps of 25 nm from 600 to 1050 nm so that images at 19 different wavelengths were taken. To avoid the ambient light modifying the contrast of the images, all of them were taken in a totally darkened laboratory.

The images were recorded as 8-bit TIFF files and processed with the Matlab package. Figure 2 shows the whole image as captured by the imaging system for $\lambda = 625$ nm. In this image, we can see the field of view and the illuminated region.

OSA CONTINUUM

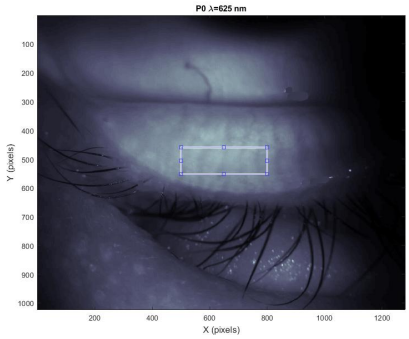

Fig. 2. 8-bit image acquired by the imaging system at wavelength λ = 625 nm for the subject P0. The rectangular region delimited by the white lines is the 300 × 90 pixels region of interest (ROI) in which the contrast is going to be measured. The ROI was the same for all the wavelengths and subjects.

In each recorded image, we selected a rectangular region of interest (ROI) with size 300 × 90 pixels for further processing (see Fig. 2). The region contained about 4 Meibomian glands with well-resolved acini (typical linear size of acini being 20 to 40 pixels). The same ROI was used in all the images. The location of the ROI was manually selected by the operator, who centered the ROI in the region where the Meibomian glands presented the greater contrast. Although it is possible to implement an automatic segmentation algorithm for selecting the zone with Meibomian glands, the extension of this zone varies from eye to eye. This is why we chose to select manually a ROI with the same extension for all the subjects. The subject was allowed to blink from image to image, and for each acquisition, the experimenter had to tune the pressure on the everted lid to avoid specular reflection from wet areas inside the ROI. Once the experimental setup was tested and ready, and all the calibrations made, the whole set of measurements (around 18 measurements, corresponding to the different wavelengths employed) was completed in a single session lasting around 60 min, so the measuring time for a single wavelength would be around 1-2 minutes. In Fig. 3 we show the ROIs obtained for the eye of the same subject (P0) illuminated with different wavelengths.

All the gland images were processed in order to obtain the intra-gland, or in-gland, contrast, and the inter-gland contrast. The in-gland contrast is the average of the Michelson's contrast measured along paths that join different acini belonging to the same gland. Michelson's contrast is defined as follows

$$C = \frac{I_{\max} - I_{\min}}{I_{\max} + I_{\min}} \tag{1}$$

where $I_{\max}$ and $I_{\min}$ are, respectively, the maximum and minimum intensities measured along a given path. Similarly, the inter-gland contrast is the average of the Michelson's contrast corresponding to pairs formed by the maximum intensity in the acini, and the minimum intensity at the regions between different glands. In all cases, the input image of the algorithm were the unprocessed ROI, as the ones shown in Fig. 3. We will describe now the main steps of the image processing algorithm employed to determine the in-gland and inter-gland contrasts.

1. The first step is the computation of the background by filtering the ROI with a 60 × 60 median filter. The median filter acts as a low pass filter by removing the fine details of the image depending on the filter's window size. For the median filter, the window size is related with the cutoff frequency of the equivalent low pass filter. Mathematically, we have that

OSA CONTINUUM

$$B(x,y) = M_{60}\left[I(x,y)\right] \tag{2}$$

where $I(x,y)$ is the intensity of the original image at the point of coordinates (x,y), $M_{60}[\ ]$ is the 60×60 median filter operator and $B(x,y)$ is the background estimation.

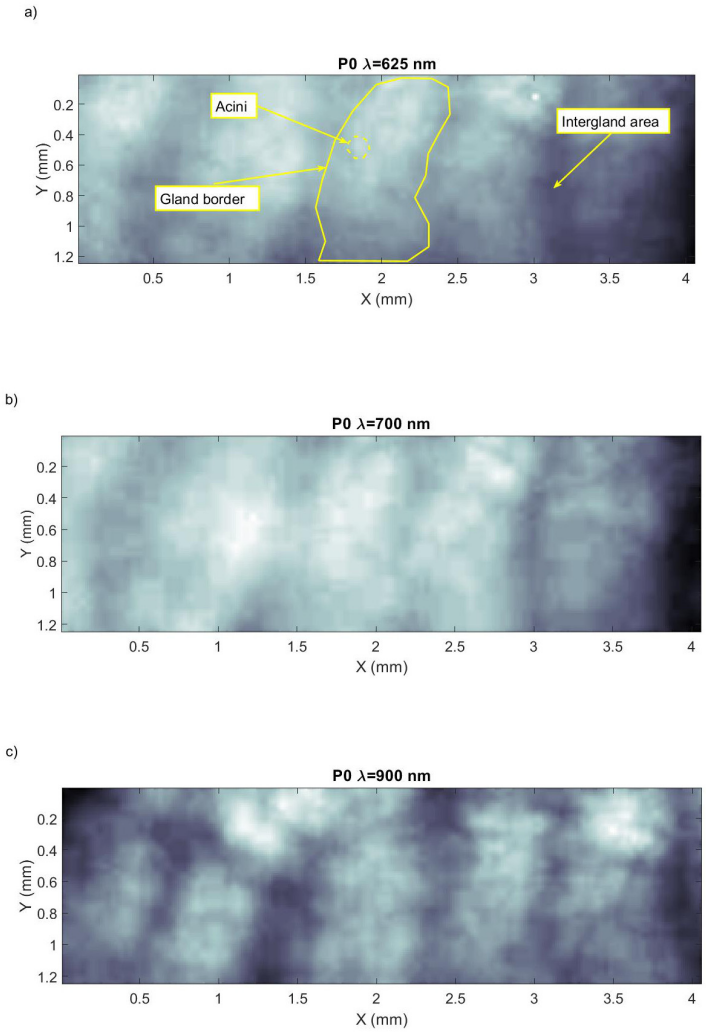

Fig. 3. ROIs obtained at three different wavelengths. (a) 625 nm, (b) 700 nm, (c) 900 nm. Notice the differences in contrast and detail between these images. In Fig. 3(a) we have indicated the different anatomical features present: the gland border, the intergland area, and one acinus.

2. The next step is the gland detection and labeling by thresholding the input image. The threshold criterion is that a point belongs to a gland if its intensity is greater than that of the background image obtained in the preceding step. The resulting binary image, or gland mask, is labeled to identify each gland separately. In Fig. 4(b) we show the image of the glands determined for the patient P0 and wavelength 625 nm as detected by the algorithm. To state the accuracy of the gland detection we have

OSA CONTINUUM

computed the total area (in square pixels) of the glands detected by the algorithm, and the area of the glands segmented manually, shown in Fig. 4(a). For the automatic glands the total area was 16028 square pixels, while the manually segmented gland mask occupied an area of 17486 square pixels, with a difference around an 8% between them. The contours of the glands detected automatically are superposed with the ones determined manually in Fig. 4(c).

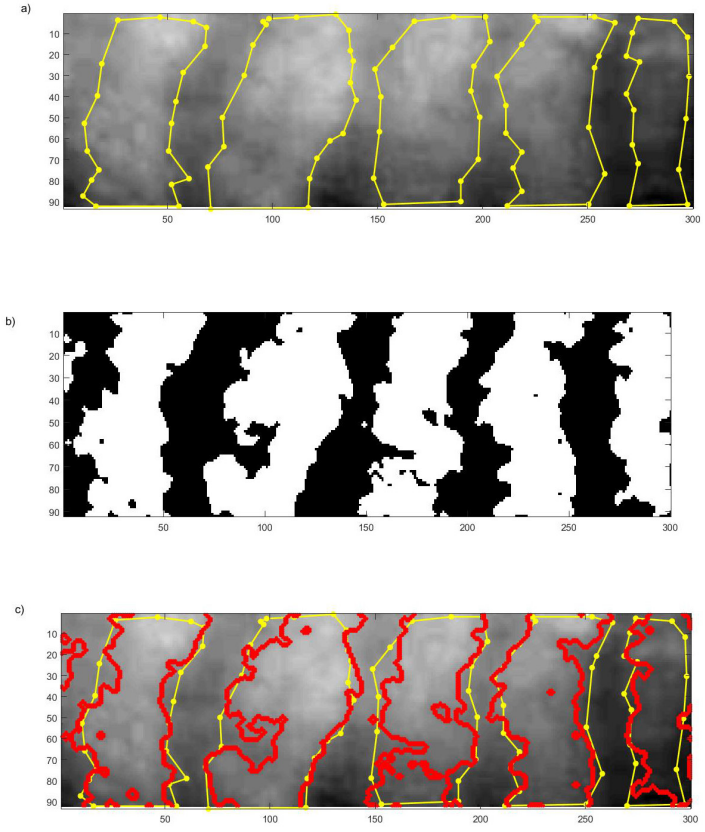

Fig. 4. (a) Image of the glands corresponding to patient P0 taken at a wavelength of 625 nm with superposed gland contours (yellow line with dots) determined manually, (b) mask of the gland detected by the algorithm, the white area are the glands and the background is black. (c) Image of the glands with the manual (yellow line) and automatic contours (red line) superposed. The automatic contours correspond with the edge of the glands shown in Fig. 4(b).

The process of gland detection can be represented by the following equation

$$M(x,y)=\begin{cases}1, & \text{if } B(x,y)\le I(x,y)\\ 0, & \text{if } B(x,y)>I(x,y)\end{cases} \tag{3}$$

being $M(x,y)$ the binary mask gland. By applying the labeling operator to the gland mask we get the label matrix as

$$L(x,y)=\mathrm{L}\left[M(x,y)\right] \tag{4}$$

OSA CONTINUUM

where $\mathrm{L}[\ ]$ is the labeling operator. This operator assigns an integer value (label) to each isolated region of the gland mask which presents 8-pixel connectivity. As a result of the labeling operator, we get a matrix of integers, known as label matrix, $L(x,y)$, which indicates whether the pixel (x,y) belongs to the background, when $L(x,y)=0$, or to a given gland when $L(x,y)=l$, being $l\in\mathbb{Z}$ the numerical value of the gland label.

3. Afterward, we search for the coordinates of pixels with maximum intensity within each acinus of each gland, using the Matlab function *imregionalmax*. The action of imregionalmax operator is given by the following equation

$$\mathrm{I}_{\mathrm{regmax}}\left[I(x,y)\right]=\left(\left\{\left(x_j,y_j\right)\right\}\middle|\, I\left(x_j,y_j\right)>I_{N_j}\ AND\ L\left(x_j,y_j\right)\neq 0\right)_{j=1,2,3\ldots M} \tag{5}$$

where I_{N_j} is the $N\times N$ neighborhood centered on the pixel with coordinates $\left(x_j,y_j\right)$, and M the total number of local maxima detected.

4. Next, we use *imregionalmin* to obtain the coordinates of the local minima for each gland. These points will usually be located in the border between two acini. Similar to the former case we have that

$$\mathrm{I}_{\mathrm{regmin}}\left[I(x,y)\right]=\left(\left\{\left(x_j,y_j\right)\right\}\middle|\, I\left(x_j,y_j\right)<I_{N_j}\ AND\ L\left(x_j,y_j\right)\neq 0\right)_{j=1,2,3\ldots R} \tag{6}$$

where I_{N_j} is the $N\times N$ neighborhood centered on the pixel with coordinates $\left(x_j,y_j\right)$, and R the total number of local maxima detected.

5. Then, we compute the in-gland contrast. To do so, we work with the unprocessed image and we compute the maximum and minimum intensity corresponding to each acinus and an inter-acini point located in steps 3 and 4. Then we form pairs of acini/inter-acini points with the following rules: (1) the two points should belong to the same gland and, (2) the distance between them should be lower than the gland width. The gland width is calculated for each gland detected using Matlab function *regionprops* which allow to compute the property 'MinorAxisLength' which, for an elongated object, like the glands, corresponds to the width of the ellipse that has the same size and orientation than the object (See further details in reference [36]). Then, we compute the Michelson's contrast for each pair and we average to get the final in-gland contrast for the whole image. Similarly, we get the standard deviation of the in-gland contrast (see Fig. 6).

   If $\left(x_j^M,y_j^M\right)$ are the coordinates of the j-th local maximum of intensity within a gland, and $\left(x_j^m,y_j^m\right)$ are the coordinates of the k-th local minimum, the conditions that should be accomplished by these points to form a valid pair of points for contrast evaluation can be stated as

$$\begin{cases} L\left(x_j^M,y_j^M\right)\equiv L\left(x_j^m,y_j^m\right)=l\neq 0, \\ \left(\left(x_j^M-x_j^m\right)^2+\left(y_j^M-y_j^m\right)^2\right)\leq w_l^2, \end{cases} \tag{7}$$

OSA CONTINUUM

being $L(x,y)$ the labeling matrix obtained in step 2 and w_l the width of the l-th gland to which the two points belong according to the upper row of Eq. (7). If the pair of points are valid, the in-gland contrast for this pair is

$$C_{jk}^{\text{in}} = \frac{I\left(x_j^M, y_j^M\right) - I\left(x_j^m, y_j^m\right)}{I\left(x_j^M, y_j^M\right) + I\left(x_j^m, y_j^m\right)} \tag{8}$$

where C_{jk}^{in} is the contrast corresponding to the pair formed by the j-th local maximum and the k-th local minimum. The average in-gland contrast, and its standard deviation, are obtained by averaging the contrast computed for all valid points.

6. Once we get the in-gland contrast, we locate the local minima of intensity at the region between glands using the high contrast images. Then, we form pairs with these points and the acini (local intensity maxima of the glands) in order to compute the inter-gland contrast. Similarly to the previous step, we validate each pair of points if the distance between them is smaller than the average gland width. In this case, if $\left(x_j^M, y_j^M\right)$ are the coordinates of a local maximum within a given gland, and $\left(x_j^m, y_j^m\right)$ is a local minimum in the inter-gland zone, they form a valid point if they accomplish the following conditions

$$\begin{cases} L\left(x_j^M, y_j^M\right) \neq 0, L\left(x_j^m, y_j^m\right) = 0, \\ \left(\left(x_j^M - x_j^m\right)^2 + \left(y_j^M - y_j^m\right)^2\right) \leq \bar{w}^2, \end{cases} \tag{9}$$

where $\bar{w}$ is the average width of all the glands detected.

7. Finally, we get the intensities corresponding to the validated acini/inter-gland point pairs, and we compute the Michelson's contrast for each pair using Eq. (1). A single inter-gland contrast figure is obtained by averaging.

OSA CONTINUUM

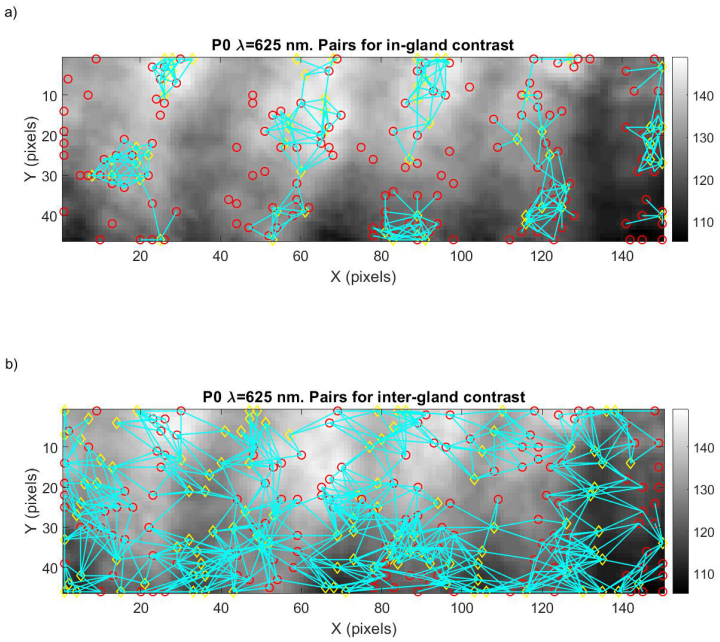

Fig. 5. (a) Plot of the acini (red circles) and inter-acini (yellow diamonds) superposed over the (unprocessed) image of the subject P0's Meibomian glands taken at 625 nm. The blue lines join the valid pairs of points, according to the criteria given in the text, from which the in-gland contrast has been determined. (b) Plot of the acini (red circles) and inter-gland points (yellow diamonds) superposed over the same ROI's. As with Fig. 5(b) the blue lines represent the valid acini/inter-gland point from which the inter-gland contrast is computed.

Figure 5(a) shows the acini and the inter-acini points detected for the ROI corresponding to subject P0 for the incident wavelength λ=625 nm. Notice that the valid points (according to the criteria given at step 5) are joined by a blue line. The in-gland contrast has been computed from these points. Also, we have displayed in Fig. 5(b) the acini and inter-gland points detected for the same ROI, also showing the valid pairs from which the inter-gland contrast has been obtained.

3. Results and discussion

We will present first the detailed results obtained for subject P0 and the averaged values of contrast for the whole sample. In Fig. 6 we have represented the values of in-gland and inter-gland contrast obtained for three different wavelengths as a box plot. In this representation, for a given set of contrast values, the red horizontal line stands for the median of the data, the upper and lower sides of the blue box are the values of contrast which correspond to the 75% and 25% percentile, respectively, the dashed segment is the range of contrast, and, finally, the red crosses are data classified as outliers.

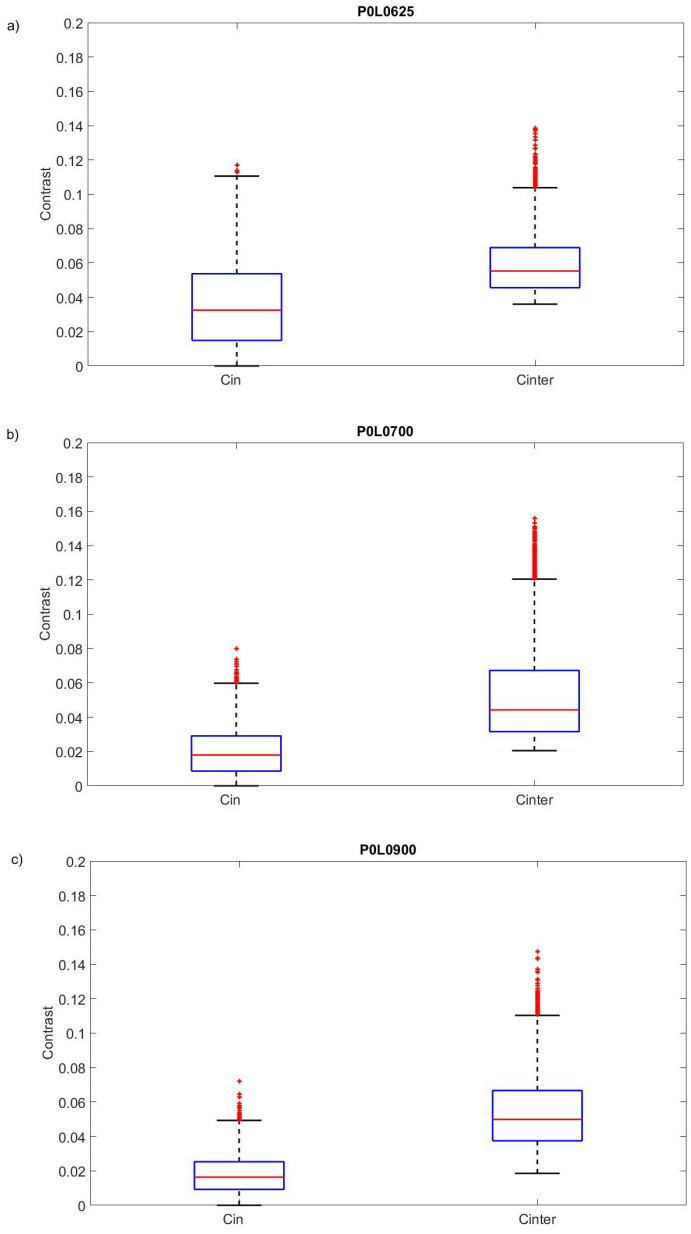

Fig. 6. Box plot representing the median (red line), the 25th and 75th percentile (bottom and top of the blue box), the range, the range of data considered as valid (dotted black interval) and the outliers red crosses) of both in-gland contrast (left) and inter-gland contrast (right). These plots have been obtained for all the valid pairs detected from the images of the lid of subject P0 shown in Fig. 3, corresponding to the wavelengths of a) 625, b) 700 and c) 900 nm.

Although the plots of Fig. 6 show a high variability for both contrasts, due to the relatively high range intervals, we can see that the box plot for inter-gland contrast is always higher than the box plot for the in-gland contrast, regardless the wavelength, indicating a difference between these contrasts. This corresponds with the subjective impression that we got when observing the images of the Meibomian glands from the same subject for the same

wavelengths (see Fig. 3) as the contrast between glands is always higher than the contrast within a gland.

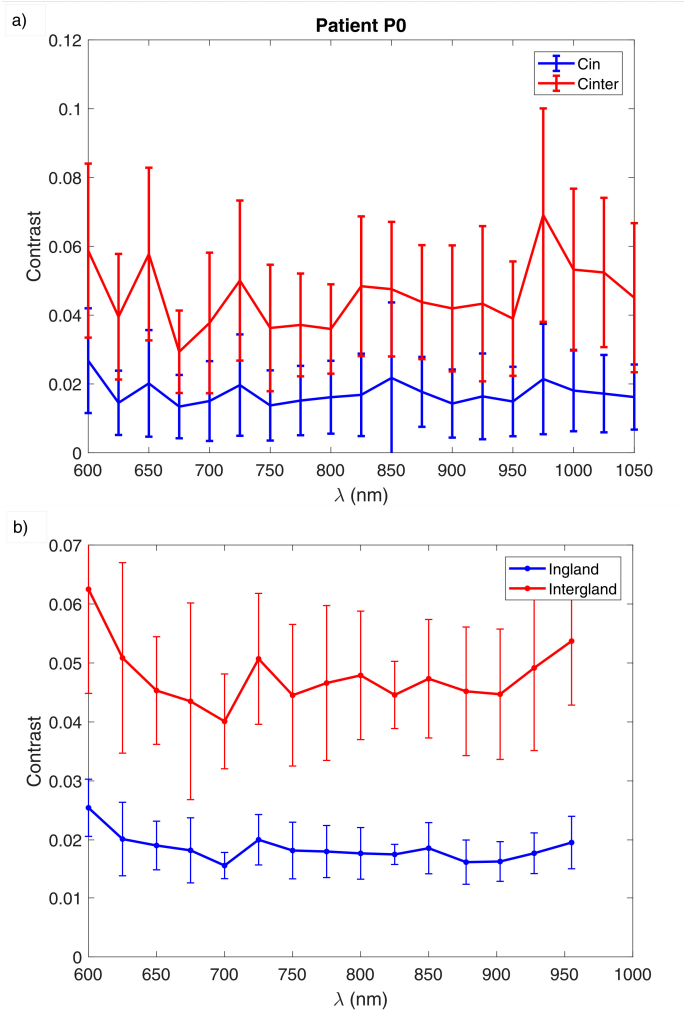

Fig. 7. (a) In-gland (blue) and inter-gland (red) contrast as a function of the wavelength. The length of the error bars is twice the value of the standard deviation. The data corresponds to the subject P0. (b) Average in-gland (blue) and inter-gland (red) contrast against the wavelength for the whole population of our study. The error bar length represents the double of the standard deviation obtained among individuals

Subjective evaluation of the ROIs in Fig. 3 suggests a larger contrast for wavelength λ=900 nm. The numerical results obtained confirm this point, as the average values for the inter-gland contrast are 0.039 for 625 nm, 0.036 for 700 nm, and 0.048 for 900 nm. On the other hand, the average in-gland contrast for these same wavelengths are 0.014, 0.015, and 0.017, respectively. However, it is worth noticing that the differences between wavelengths are quite low.

Figure 7(a) shows the averaged inter-gland and in-gland contrasts for subject P0 as a function of the wavelength of the incident light. The difference between in-gland and inter-gland contrasts observed for the three wavelengths presented in Fig. 7(a), keeps approximately the same for all the wavelengths, with values around 0.05 for inter-gland contrast and values around 0.02 for in-gland contrast.

OSA CONTINUUM

In Fig. 7(b) we present a plot of the in-gland and inter-gland contrast, averaged for all the 10 subjects as a function of wavelength. Similar values of inter-gland and in-gland contrast are observed in the subject average so the difference between both is still 0.03. Considering that all of the subjects of our study presented healthy eyes and were not users of contact lenses, it seems that the basal values of the inter-gland and in-gland contrast for a healthy individual are 0.05 and 0.02, respectively.

Apparently, from Fig. 7(b) there is some correlation between maxima and minima of the in-gland and inter-gland contrast with wavelength. According to these curves, there are three optimal wavelengths for Meibomian gland observation: the edges of the explored spectral range, (600 and 950 nm) and a small peak centered at the wavelength 725 nm. Notice that we have restricted the wavelength interval from 600 to 950 nm as we were not able to obtain good images (images with enough contrast to distinguish the Meibomian glands) for some subjects at wavelengths longer than 950 nm.

In order to test whether there is a dependence between the average in- and inter-gland contrasts with the wavelength, we fitted the data to different functions. However, due to the high variability of the data, we did not find a reliable fit. Therefore, we have used contrast hypothesis tests in order to determine whether the measured contrast is higher for the extreme wavelengths of the spectral region studied, particularly for the red end. This is a relevant question because the usage of a red wavelength permits simpler and cheaper experimental set-ups as there is no need for IR sources. In particular, it would eventually allow the usage of mobile devices such as tablets, cell phones, etc. to take the images.

Therefore, we have performed a hypothesis contrast in order to check whether the mean value of the contrast measured for a low wavelength (600 nm) is greater than the mean value for an intermediary wavelength (775 nm). We have used the Welch's unequal variances t-test for comparing two normally distributed populations with different means and variances. Using this test, we got a positive result for the inter-gland contrast as the null hypothesis (the mean values of contrast for the wavelengths of 600 and 775 nm are equal) was rejected by the test within a significance level of 0.05. For the in-gland contrast, the Welch's t-test was not applicable as the previous normality check of the samples (using the Lilliefors test with a significance level of 0.01) for the two wavelengths studied failed. Therefore we have performed a non-parametric Wilcoxon-Mann-Whitney test to check whether the null hypothesis that the median values of the in-gland contrast for the wavelengths of 600 and 775 nm are equal. In this case the null hypothesis was rejected at a significance level of 5%. The significance of this results is that it is possible to get more contrast when illuminating the eyelid with a wavelength close to 600 nm.

4. Conclusions

In this work, we have carried out an experiment for determine the contrast of Meibomian glands from the images of the inner side of the eyelids captured when illuminated with different wavelengths. To do so, we have employed an image processing algorithm based on the detection of local maxima and minima of intensity within the glands and within the inter gland regions. We have measured ten subjects with healthy eyes in order to determine the average change of the contrast with the wavelength.

The local contrast presents high variability for a given wavelength and a given individual. However, the algorithm employed evaluates the contrast at a large number of locations within the ROI, yielding an average contrast value, albeit with still a considerable variance. Regardless of the wavelength, there is always a significant difference between the inter- and in-gland contrasts, being systematically greater the former than the latter. The variability of the averaged contrasts across individuals is smaller than the variability of the local contrasts for any given individual. As a future work, an important effort should be made in order to improve the quality of the data obtained, with particular emphasis on the control and reduction of variance.

OSA CONTINUUM

Finally, regarding the dependence of contrast with wavelength, the edges of the scanned spectral range are preferable for Meibomian gland inspection as they deliver 30 to 40% more contrast than the remaining red and infrared wavelengths. Although we have not been able to find a model that fits properly the average contrast against wavelength, we have found with statistical significance that the average inter and in-gland contrast for a low wavelength (600 nm) is greater than the one found at an intermediate wavelength (775 nm). Apparently, it seems that the contrast curves could keep growing below 600 nm and above 950 nm, but going beyond these thresholds is not advisable. For visible light, the contrast of Meibomian glands rapidly deteriorates for wavelengths shorter than 600 nm. Besides, other structures as capillaries will appear, disrupting the images of the glands. For wavelengths longer than 950 nm contrast seems to keep growing, but the efficiency of standard CCD or CMOS sensors gets too small, with the subsequent increment of the signal to noise ratio.

The contrast of the images of Meibomian glands associated with healthy eyes is precisely quantified for the first time. The results obtained open the possibility of using the contrast of Meibomian gland images as an indicator or even a quantifier of Meibomian gland dysfunction although this will require measuring a large number of subjects with or without Meibomian gland dysfunction which is outside the scope of the present work.

Funding

European Fund for Regional Development (EFRD-FEDER, EU); Spanish Government Agencia Estatal de Investigación (DPI2016-75272-R).

References

1. N. Knop and E. Knop, “Meibomian glands. part I: anatomy, embryology and histology of the Meibomian glands,” Ophthalmologe **106**(10), 872–883 (2009).
2. B. Nagyová and J. M. Tiffany, “Components responsible for the surface tension of human tears,” Curr. Eye Res. **19**(1), 4–11 (1999).
3. J. P. Craig and A. Tomlinson, “Importance of the lipid layer in human tear film stability and evaporation,” Optom. Vis. Sci. **74**(1), 8–13 (1997).
4. T. J. Millar and B. S. Schuett, “The real reason for having a meibomian lipid layer covering the outer surface of the tear film - A review,” Exp. Eye Res. **137**, 125–138 (2015).
5. C. F. Cerretani, N. H. Ho, and C. J. Radke, “Water-evaporation reduction by duplex films: application to the human tear film,” Adv. Colloid Interface Sci. **197-198**, 33–57 (2013).
6. E. Knop, N. Knop, H. Brewitt, U. Pleyer, P. Rieck, B. Seitz, and F. Schirra, “Meibomian glands: part III. dysfunction - argument for a discrete disease entity and as an important cause of dry eye,” Ophthalmologe **106**(11), 966–979 (2009).
7. G. N. Foulks and A. J. Bron, “Meibomian gland dysfunction: a clinical scheme for description, diagnosis, classification, and grading,” Ocul. Surf. **1**(3), 107–126 (2003).
8. K. K. Nichols, G. N. Foulks, A. J. Bron, B. J. Glasgow, M. Dogru, K. Tsubota, M. A. Lemp, and D. A. Sullivan, “The international workshop on Meibomian gland dysfunction: executive summary,” Invest. Ophthalmol. Vis. Sci. **52**(4), 1922–1929 (2011).
9. A. Heiligenhaus, J. M. Koch, F. E. Kruse, C. Schwarz, and T. N. Waubke, “Diagnosis and and differentiation of dry eye disorders,” Ophthalmologe **92**(1), 6–11 (1995).
10. E. Knop and N. Knop, “Meibomian glands: part IV. functional interactions in the pathogenesis of Meibomian gland dysfunction (MGD),” Ophthalmologe **106**(11), 980–987 (2009).
11. J. D. Nelson, J. Shimazaki, J. M. Benitez-del-Castillo, J. P. Craig, J. P. McCulley, S. Den, and G. N. Foulks, “The international workshop on Meibomian gland dysfunction: report of the definition and classification subcommittee,” Invest. Ophthalmol. Vis. Sci. **52**(4), 1930–1937 (2011).
12. R. Tapie, “Etude biomicroscopique des glandes de Meibomius,” Ann. Ocul. (Paris) **210**(9), 637–648 (1977).
13. J. V. Jester, L. Rife, D. Nii, J. K. Luttrull, L. Wilson, and R. E. Smith, “In vivo biomicroscopy and photography of Meibomian glands in a rabbit model of Meibomian gland dysfunction,” Invest. Ophthalmol. Vis. Sci. **22**(5), 660–667 (1982).
14. J. B. Robin, J. V. Jester, J. Nobe, N. Nicolaides, and R. E. Smith, “Invivo trans-illumination biomicroscopy and photography of Meibomian gland dysfunction. a clinical study,” Ophthalmology **92**(10), 1423–1426 (1985).
15. W. D. Mathers, “Ocular evaporation in Meibomian gland dysfunction and dry eye,” Ophthalmology **100**(3), 347–351 (1993).
16. W. D. Mathers, W. J. Shields, M. S. Sachdev, W. M. Petroll, and J. V. Jester, “Meibomian gland morphology and tear osmolarity: changes with Accutane therapy,” Cornea **10**(4), 286–290 (1991).

OSA CONTINUUM

17. N. Yokoi, A. Komuro, H. Yamada, K. Maruyama, and S. Kinoshita, "A newly developed video-meibography system featuring a newly designed probe," Jpn. J. Ophthalmol. **51**(1), 53–56 (2007).
18. W. D. Mathers, T. Daley, and R. Verdick, "Video imaging of the Meibomian gland," Arch. Ophthalmol. **112**(4), 448–449 (1994).
19. J. J. Nichols, D. A. Berntsen, G. L. Mitchell, and K. K. Nichols, "An assessment of grading scales for meibography images," Cornea **24**(4), 382–388 (2005).
20. R. Arita, K. Itoh, K. Inoue, and S. Amano, "Noncontact infrared meibography to document age-related changes of the Meibomian glands in a normal population," Ophthalmology **115**(5), 911–915 (2008).
21. R. Arita, K. Itoh, S. Maeda, K. Maeda, A. Furuta, S. Fukuoka, A. Tomidokoro, and S. Amano, "Proposed diagnostic criteria for obstructive Meibomian gland dysfunction," Ophthalmology **116**(11), 2058–2063 (2009).
22. R. Arita, K. Itoh, S. Maeda, K. Maeda, A. Tomidokoro, and S. Amano, "Efficacy of diagnostic criteria for the differential diagnosis between obstructive Meibomian gland dysfunction and aqueous deficiency dry eye," Jpn. J. Ophthalmol. **54**(5), 387–391 (2010).
23. R. Arita, K. Itoh, K. Inoue, A. Kuchiba, T. Yamaguchi, and S. Amano, "Contact lens wear is associated with decrease of Meibomian glands," Ophthalmology **116**(3), 379–384 (2009).
24. Y. Matsumoto, Y. Shigeno, E. A. Sato, O. M. A. Ibrahim, M. Saiki, K. Negishi, Y. Ogawa, M. Dogru, and K. Tsubota, "The evaluation of the treatment response in obstructive Meibomian gland disease by in vivo laser confocal microscopy," Graefes Arch. Clin. Exp. Ophthalmol. **247**(6), 821–829 (2009).
25. H. Pult and B. H. Riede-Pult, "Non-contact meibography: keep it simple but effective," Cont. Lens Anterior Eye **35**(2), 77–80 (2012).
26. S. Srinivasan, K. Menzies, L. Sorbara, and L. Jones, "Infrared imaging of Meibomian gland structure using a novel keratograph," Optom. Vis. Sci. **89**(5), 788–794 (2012).
27. P. E. Napoli, F. Coronella, G. M. Satta, C. Iovino, R. Sanna, and M. Fossarello, "A simple novel technique of infrared meibography by means of spectral-domain optical coherence tomography: a cross-sectional clinical study," PLoS ONE **11**(10), e0165558 (2016).
28. S. C. Pflugfelder, S. C. Tseng, O. Sanabria, H. Kell, C. G. Garcia, C. Felix, W. Feuer, and B. L. Reis, "Evaluation of subjective assessments and objective diagnostic tests for diagnosing tear-film disorders known to cause ocular irritation," Cornea **17**(1), 38–56 (1998).
29. L. C. McCann, A. Tomlinson, E. I. Pearce, and C. Diaper, "Tear and Meibomian gland function in blepharitis and normals," Eye Contact Lens **35**(4), 203–208 (2009).
30. H. Pult, B. H. Riede-Pult, and J. J. Nichols, "Relation between upper and lower lids' Meibomian gland morphology, tear film, and dry eye," Optom. Vis. Sci. **89**(3), E310–E315 (2012).
31. H. Pult and B. Riede-Pult, "Comparison of subjective grading and objective assessment in meibography," Cont. Lens Anterior Eye **36**(1), 22–27 (2013).
32. W. D. Mathers, W. J. Shields, M. S. Sachdev, W. M. Petroll, and J. V. Jester, "Meibomian gland dysfunction in chronic blepharitis," Cornea **10**(4), 277–285 (1991).
33. T. Celik, H. K. Lee, A. Petznick, and L. Tong, "Bioimage informatics approach to automated Meibomian gland analysis in infrared images of meibography," J. Optom. **6**(4), 194–204 (2013).
34. R. Koprowski, S. Wilczyński, P. Olczyk, A. Nowińska, B. Węglarz, and E. Wylęgała, "A quantitative method for assessing the quality of Meibomian glands," Comput. Biol. Med. **75**, 130–138 (2016).
35. R. Koprowski, L. Tian, and P. Olczyk, "A clinical utility assessment of the automatic measurement method of the quality of Meibomian glands," Biomed. Eng. Online **16**(1), 82 (2017).
36. The MathWorks Inc, "Regionprops. Measure properties of image region" Matlab R2018a documentation, *https://es.mathworks.com/help/images/ref/regionprops.html#buoixjn-3*, (2018).